

Effects of size and shape on electronic states of quantum dots

C. Y. Ngo, S. F. Yoon, and W. J. Fan

School of Electrical and Electronic Engineering, Nanyang Technological University, Nanyang Avenue, Singapore 639798, Republic of Singapore

S. J. Chua

Faculty of Engineering, Institute of Materials Research and Engineering, 3 Research Link, Singapore 117602, Republic of Singapore

(Received 3 January 2006; published 29 December 2006)

A strained-modified, single-band, constant-potential three-dimensional model is formulated to study the dependence of electronic states of InAs/GaAs quantum dots (QDs) on shape and size variation. The QD shapes considered are (i) cuboid, (ii) cylindrical, (iii) pyramidal, (iv) conical, and (v) lens shaped. Size variations include (i) QD volume (ii) QD base length, and (iii) QD height, taking into account aspect ratio variation. Isovolume QD shapes with narrow tips were found to have higher ground-state energies than those with broad tips, and this is attributed to the smaller effective volume. The volume, base length, and height dependencies were obtained and found to tally well with both experimental results and advanced calculations. Hence, upon growth parameter variation, this can provide an alternative to confirm whether the change to the size of the uncapped QDs implies a similar change to the capped ones. Ground-state energy as function of aspect ratio does not follow a monotonic trend. Owing to the competing effect of a decrease in base length and an increase in height, the energy trend exhibits a sharp decrease to an optimum aspect ratio, followed by gentle, almost linear increase. The optimum aspect ratio varies among shapes and is predicted to be smaller for shapes with broad tips. The effective volume ratio of both shapes ($V_{\text{eff,CUBOID}}/V_{\text{eff,PYRAMID}}$) was determined, and found to vary with aspect ratio. Furthermore, a “cross-over” of lens-shaped QD from “lower energy” to “higher energy” group is predicted due to significant shape transition.

DOI: [10.1103/PhysRevB.74.245331](https://doi.org/10.1103/PhysRevB.74.245331)

PACS number(s): 68.65.Hb, 73.21.La

I. INTRODUCTION

Semiconductor research and development has seen progressive reduction in dimension, from bulk material to quantum well, then to quantum wire, and eventually to quantum dot (QD). Being the ultimate limit in carrier confinement, semiconductor QDs are the center of research attention due to their unique electronic and optical properties. This is due to their three-dimensional (3D) carrier confinement property, thus bringing with them superior characteristics of atomlike density-of-states (DOS), large exciton binding energies, and enhanced oscillator strength.

These desired properties of quantum dots have spun new research in various QD devices, e.g., laser, infrared photodetector (QDIP), and electroabsorption modulator (EAM). However, as there are specific requirements for different QD devices, there is a need to alter the dimensions of the active material to suit the requirements. For example, larger QDs (and thus lower transition energy) are required for long wavelength emission and detection, taller QDs (and thus larger confinement in the growth direction) will exhibit larger quantum confined stark effect (QCSE), and smaller QDs (with single confined state) are useful for quantum computing for single photon emission and detection. Furthermore, the energy difference between ground-state energy and excited-state energy is important for carrier dynamics (e.g., relaxation time for laser and escape time for detector) and is of great concern for high-speed device operation.

Presently, by growing an uncapped QD at the top of the growth structure, atomic force microscopy (AFM) is conveniently being used to provide a fast feedback loop upon growth parameters variations. However, due to the difference

in growth structures and procedures after the QD growth (capping materials, annealing time and temperature, etc.), capped QDs can be significantly different from the uncapped ones. The current way to check them will then be the use of sophisticated tools such as the high resolution transmission electron microscope (HREM). Thus, it is desirable to find an easier way to determine the amount of size deviation of the capped QD from the uncapped QD upon a growth parameter variation.

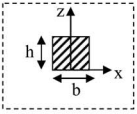
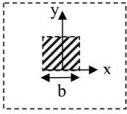
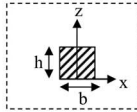
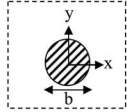
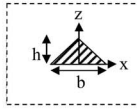
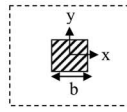
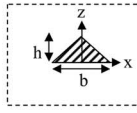
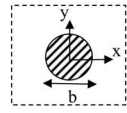
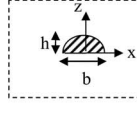
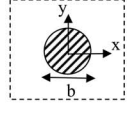
In practice, the QD shape and size will exert a significant influence on its electronic structure, optical property and hence wavelength characteristic. Presently, data on cuboid,¹ cylindrical,^{2,3} pyramidal,^{4–16} conical,^{4,17–19} and lens-shaped^{1,15,20–22} QDs have been published in literature. However, most of the electronic structure calculations in present literature were performed based on a fixed QD shape and size. To date, there is limited data on the effects of QD shape and size variations on its electronic states.

This paper presents our work on the electronic states of InAs/GaAs QDs and the effect of shape and size variation. Our study aims to understand the energy trends as a function of QD shape and size, to obtain the energy dependency on each QD dimension variation, and thus to apply that knowledge to investigate an easier method for determining the amount of size deviation of the capped QDs from the uncapped ones.

II. MODELS

Table I illustrates the various QD shapes considered in this study, namely, the cuboid, cylindrical, pyramidal, conical,

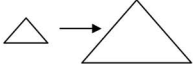
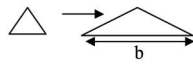
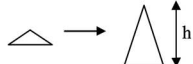
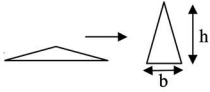
TABLE I. Quantum dot shapes considered.

QD shape		Name (Abbreviation)	Boundary definition and volume
Cross section	Plan view		
		Cuboid QD (CUBOID)	$ x \leq b/2$ $ y \leq b/2$ $0 \leq z \leq h$ $V_{\text{CUBOID}} = hb^2$
		Cylindrical QD (CYLINDER)	$(x^2 + y^2) \leq (b/2)^2$ $0 \leq z \leq h$ $V_{\text{CYLINDER}} = (\pi/4)hb^2$
		Pyramidal QD (PYRAMID)	$ x \leq [b(h-z)]/2h$ $ y \leq [b(h-z)]/2h$ $V_{\text{PYRAMID}} = (1/3)hb^2$
		Conical QD (CONE)	$(x^2 + y^2) \leq \{(b/2)[(h-z)/h]\}^2$ $V_{\text{CONE}} = (\pi/12)hb^2$
		Lens-shaped QD (LENS)	$(x^2 + y^2) \leq [r_s^2 - (r_s - h - z)^2]$ $r_s = (4h^2 + b^2)/8h$ $V_{\text{LENS}} = (\pi h/24)(4h^2 + 3b^2)$

cal, and lens shaped. The cross-sectional and plan views of these QD shapes are shown and identified by their abbreviations. The different boundary conditions for performing the band structure calculation are indicated in the table. Note that cubic is a special case of CUBOID (i.e., when $h=b$).

Table II illustrates the physical parameters considered in this study, namely, the volume (Vol.), base length (b), height (h), and aspect ratio (AR). As QD volume is varied, aspect ratio of all QD shapes is fixed at 0.5 (i.e., $\text{AR}=0.5$), so that the height-to-base ratio is kept constant throughout. The

TABLE II. Physical parameters considered.

Parameter	Abbreviation	Parameter range	Illustration
QD Volume	Vol.	$10^4 - 10^7 \text{ \AA}^3$	
QD Base	b	$50 - 400 \text{ \AA}$	
QD Height	h	$20 - 140 \text{ \AA}$	
QD aspect ratio $= \frac{\text{QD height}}{\text{QD base length}}$	$\text{AR} = h/b$	$0.1 - 2$	

range of volume variation (from 10^4 to 10^7 Å³) is considered realistic, as these translate to a base of ~ 50 Å and height ~ 25 Å (as shown in Refs. 1 and 2) to a base of ~ 400 Å and height of ~ 200 Å, respectively. The relatively high upper limit dimensions are investigated to provide an insight into the effect on electronic states at high QD volumes.

The QD height was maintained at 25 Å as the base length is varied. This is to isolate the effect of height and focus on the impact of base length variation on the energy states. Likewise, for the case of height variation, the base length was fixed at 250 Å as the height is varied, so as to isolate the effect of base and focus on the impact due to height variation. Likewise, the high upper limit dimensions are to provide an insight into the effect on electronic states at high QD base or height dimensions.

To investigate the effect of QD aspect ratio (AR) variation, the volume of all QD shapes was fixed at 8×10^5 Å³. This will allow us to focus on the effect of AR changes on the energy states as the volume is held constant. This volume is again realistic as it translates to QD base of ~ 280 Å and QD height of ~ 28 Å (as reported in Refs. 4 and 22). Interestingly, as QD aspect ratio increases, the QD will undergo a “transformation” from one of larger base and shorter height to one of smaller base and taller height (as shown in Table II). This leads to the question of how the energy states will change as the aspect ratio is varied, i.e., as the base length decreases and height increases. We know that bound state energies increase following increase in confinement. Hence, the question lies in whether bound energies will increase (since base length decreases, implying a larger lateral confinement) or decrease (since height increases, implying a smaller vertical confinement) in such cases.

The authors recognized that it is not common to have QDs with $AR > 0.5$. Nevertheless, the upper AR limit of 2.0 was investigated to reveal other possible observations; and this will be discussed in Sec. III. Such observations may be useful for growth techniques that are capable of producing $AR > 0.5$, e.g., templated QD growth.

The single-band effective-mass approximation to Schrödinger's equation has been used to calculate the electron and heavy-hole energy levels. Comparisons between single-band, eight-band $\mathbf{k} \cdot \mathbf{p}$ and (the more accurate) direct-diagonalization empirical-pseudopotential-method (DD-EPM) were reported in Ref. 11. It was shown that the commonly used eight-band $\mathbf{k} \cdot \mathbf{p}$ model did not fare significantly better in terms of accuracy for determining the electronic band structure. The ground-state energy calculated by the single-band model (1103 meV) gave a value of 144 meV (15%) higher than that given by the DD-EPM method (959 meV). The eight-band $\mathbf{k} \cdot \mathbf{p}$ model (1045 meV) gave a value of 86 meV (8%) higher, despite its greater computational complexity compared to the single-band model. The simplicity in the calculation and computational efforts, and the fact that the result from the single-band model only differed by $\sim 5.5\%$ from that of the eight-band $\mathbf{k} \cdot \mathbf{p}$ model thus makes it very attractive. Hence, the single-band model is used in this study to investigate the dependence of the electronic states with respect to the physical variations illustrated in Tables I and II.

Within the framework of the envelope function and effective mass theory, the Hamiltonian can be written as

$$H = \frac{-\hbar^2}{2} \nabla \frac{1}{m^*(x,y,z)} \nabla + V(x,y,z) \quad (1)$$

where

$$m^*(x,y,z) = \begin{cases} m_{InAs}^*, & \text{in QD} \\ m_{GaAs}^*, & \text{otherwise,} \end{cases}$$

$$V(x,y,z) = \begin{cases} 0, & \text{in QD} \\ \Delta E_V \text{ or } \Delta E_C, & \text{otherwise,} \end{cases}$$

where m_{InAs}^* , m_{GaAs}^* are the effective mass of carriers in InAs and GaAs, respectively. ΔE_V and ΔE_C are the valence band and conduction band discontinuity, respectively.

Assuming that the wave functions are expanded in terms of normalized plane waves,

$$\psi(x,y,z) = \frac{1}{\sqrt{L_x L_y L_z}} \sum_{n_x, n_y, n_z} a_{n_x, n_y, n_z} e^{i(k_{n_x}x + k_{n_y}y + k_{n_z}z)}, \quad (2)$$

where L_x , L_y , L_z are lengths of the unit cell along the x , y , and z directions, respectively; n_x , n_y , n_z are the number of plane waves along the x , y , and z directions, respectively; $k_{n_x} = k_x + n_x K_x$, $K_x = 2\pi/L_x$; $k_{n_y} = k_y + n_y K_y$, $K_y = 2\pi/L_y$; and $k_{n_z} = k_z + n_z K_z$, $K_z = 2\pi/L_z$.

As reported,²³ the attraction of the normalized plane-wave approach lies in the fact that there is no need to explicitly match the wave functions across the boundary of the barrier and QD materials. Hence, this method is easily applied to an arbitrary confining potential problem.

The electron and hole energy states were calculated using the discretized Schrödinger's equation technique. As such, this method is useful for treating problems with complex geometry. The main drawback of this technique lies in the possible errors involved in the large computation. The authors are aware of this and steps were taken to ensure the errors involved in the calculation are as small as possible, typically less than 0.001%.

Seven normalized plane waves in each direction were used to form the Hamiltonian matrix, i.e., with n_x , n_y , n_z each ranging from -3 to 3 . Hence, a 343×343 matrix is formed, and the energy eigenvalues and eigenfunctions can be solved using relatively modest computing resources. By taking more plane waves, e.g., n_x , n_y , n_z each ranging from -4 to 4 , a 729×729 matrix can be formed that gives more accurate results. However, it was found that since the difference in the calculated results between using the 343×343 matrix and 729×729 matrix was only ~ 1 meV, the significantly longer computation time involved by using the larger dimension matrix does not justify using a basis of nine normalized plane waves in each direction. Therefore, only seven normalized plane waves in each direction have been considered.

The parameters listed in Table III (Refs. 8 and 23–27) were used in the calculation, and the results will be discussed in Sec. III. The strain in the InAs layer and GaAs barrier layer was considered as constant and zero, respectively, implying a constant confining potential. In addition, the strained-modified InAs band gap was used in the calculation. Some reports^{28,29} have indicated two different values for the hole effective mass, namely, $m_{hh,z}^*$ and $m_{hh,xy}^*$ along the z

TABLE III. Parameters used in the calculations.

Parameters	Unit	Values
$m_{e(\text{GaAs})}^*$	m_0	0.0665
$m_{e(\text{InAs})}^*$	m_0	0.04
$m_{hh(\text{GaAs})}^*$	m_0	0.377
$m_{hh(\text{InAs})}^*$	m_0	0.590
$E_{g\text{GaAs}}$	eV	1.424
$E_{g\text{InAs}}$	eV	0.720
$\Delta E_C/(E_{g\text{GaAs}}-E_{g\text{InAs}})$	-	0.54
$\Delta E_V/(E_{g\text{GaAs}}-E_{g\text{InAs}})$	-	0.46

direction and xy plane, respectively, to account for mass anisotropy. However, this increases the computational effort without significant improvement to the results (2.5% difference as calculated by Grundmann *et al.*²⁸). Hence, we chose to use a single value for the hole effective mass, which is $0.59m_0$. This value was proven to reproduce well the ground-state energies considered in Ref. 12.

We have chosen to exclude the wetting layer since this paper aims to investigate the impact of parameter variation on the electronic states. Hence, when a particular parameter is varied, we would aim to reduce and, if possible, isolate the effect of remaining parameters on the electronic states. We have also ignored additional effects, such as potential due to piezoelectricity, Coulombic interaction, and strain distribution within the QD. The effect of piezoelectric potential is ignored since its effect on the energy levels involved in optical transitions is only marginal²⁸ (<1 meV). Furthermore, the QDs considered in this paper are within the strong confinement regime, i.e., the effective radius is much smaller compared to the bulk exciton Bohr radius. Therefore, Coulombic interaction effects can be ignored.^{30,31} Strain distribution was reported to depend primarily on the QD shape and not QD size.²⁸ Therefore, while different QD shapes result in different strains within the QD, thus leading to different confining potentials and effective masses, the strain distribution for any given shape should be similar. Hence, the study of QD size variation should reveal the true trend for the energy states. Furthermore, the strain distribution in the major part of the QD structure is very similar for different shapes,³² especially since the hydrostatic component depends weakly on the QD shape. Therefore, even though our model did not incorporate the complexities to account for the above additional effects, it still retains key elements of the essential physics.

III. RESULTS AND DISCUSSION

This section discusses the results and physics behind the observed trends as the physical parameters are varied. In all the figures illustrated in this section, the electron energy states are taken with respect to the InAs conduction band, while the heavy-hole energy states are taken with respect to the InAs valence band. All energies are in unit of meV and dimensions are in unit of Å.

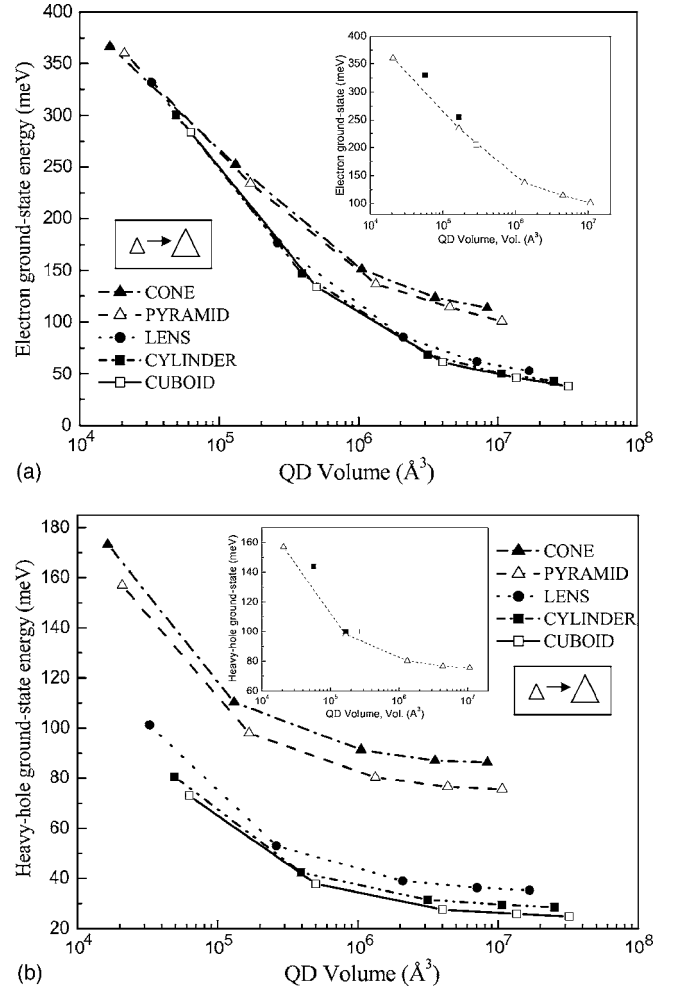


FIG. 1. Plot of (a) electron ground-state energy and (b) heavy-hole ground-state energy as function of QD volume, for various QD shapes (QD aspect ratio fixed at 0.5). The lines are guides to the eyes. (Inset) Validation of our model (hollow triangles with dotted line) for InAs/GaAs pyramidal QDs against the theoretical models from Cusack *et al.* (hollow squares) and Grundmann *et al.* (filled squares).

A. QD volume variation

The prediction of decrease in the energy states following increase in the QD dimension can be understood from reduction in the quantum confinement. Analytically, it can be inferred from equations (A5), (A7), and (A8) in the Appendix for the case of volume, base length, and height variations, respectively. The electron ground-state energies of various QD shapes, as function of QD volume, are shown in Fig. 1(a), while the heavy-hole ground-state energies are shown in Fig. 1(b). In addition, the insets in Figs. 1(a) and 1(b) show the validation of our model (hollow triangles with dotted line) for InAs/GaAs pyramidal QDs against the theoretical models from Cusack *et al.*²³ (hollow squares) and Grundmann *et al.*²⁸ (filled squares). In this case, all the pyramidal QD shapes have a fixed aspect ratio of 0.5 and both Cusack *et al.* and Grundmann *et al.* have calculated the bound energy states with multiband models that account for strain and piezoelectric effect. The small energy discrepancy

TABLE IV. Calculated volume dependency for electron ($\gamma_{\text{electron}}^{\text{calc}}$) and hole ($\gamma_{\text{hole}}^{\text{calc}}$) energy states for PYRAMID and CUBOID.

	$\gamma_{\text{electron}}^{\text{calc}}$	$\gamma_{\text{hole}}^{\text{calc}}$
PYRAMID	0.24	0.57
CUBOID	0.40	0.61

is reasonable, considering the assumptions made in our single-band model.

Despite similar decreasing trend, there is an obvious energy difference between isovolume QD shapes. In general, it can be divided into two groups, with CONE and PYRAMID having higher energy states while CUBOID, CYLINDER, and LENS having lower energy states. As shown in Eq. (A5) in the Appendix, $E \sim V^{-\gamma}$ with $\gamma=2/3$ for the CUBOID QD with infinite barrier. Hence, to investigate this energy difference, we aim to find the volume dependency γ of the two distinct groups by fitting our results from the electron and heavy-hole energy states. The pyramidal shape is taken to represent the “higher energy” group and the CUBOID shape is taken to represent the “lower energy” group. The CUBOID shape also allows us to differentiate the real case of a finite energy barrier from the ideal case of infinite energy barrier as discussed in the Appendix.

Table IV shows the volume dependency for electron ($\gamma_{\text{electron}}^{\text{calc}}$) and hole ($\gamma_{\text{hole}}^{\text{calc}}$) energy states for PYRAMID and CUBOID. As seen from the table, the values of $\gamma_{\text{hole}}^{\text{calc}}$ are closer to the ideal case of ~ 0.67 , while that of $\gamma_{\text{electron}}^{\text{calc}}$ differ significantly. This is due to the heavier hole mass. Hence, the holes are more confined and the energy barrier seen by the holes at the ground-state energy is much larger and approximately equals that of an infinite energy barrier. In addition, $\gamma_{\text{electron}}^{\text{calc}}$ for PYRAMID is much smaller than that of CUBOID. In fact, $\gamma_{\text{hole}}^{\text{calc}}$ for PYRAMID also shows weaker volume dependency, but the difference is relatively smaller due to the heavier mass. We believe that, despite the same QD volume, the *effective* volume of the pyramidal shape is actually smaller than that of the CUBOID shape. From Eq. (A6), it is known that the energy spacing between the first excited-state energy and ground-state energy is volume dependent. Following this, we present in Fig. 2 the plot of electron ground-state energy and first excited-state energy as a function of QD volume for PYRAMID and CUBOID. Indeed, it was noted that the decrease in energy spacing is more significant for CUBOID, implying a larger increase in the effective volume compared to PYRAMID. This validates our above-mentioned reason regarding the difference in the effective volume for different shapes. In fact, similar trends were observed for the remaining shapes (i.e., CONE is similar to PYRAMID, while Lens and Cylinder are similar to CUBOID) of the two groups. Thus, we believe that for QDs of the same volume, those with narrow tips (e.g., pyramidal shape) will have a higher energy state compared to those with broad tips (e.g., lens shape). As mentioned, this is due to smaller effective volume in QDs with narrow tips.

To validate our explanation, we compared our calculated results with experimental data for different QD shapes. There

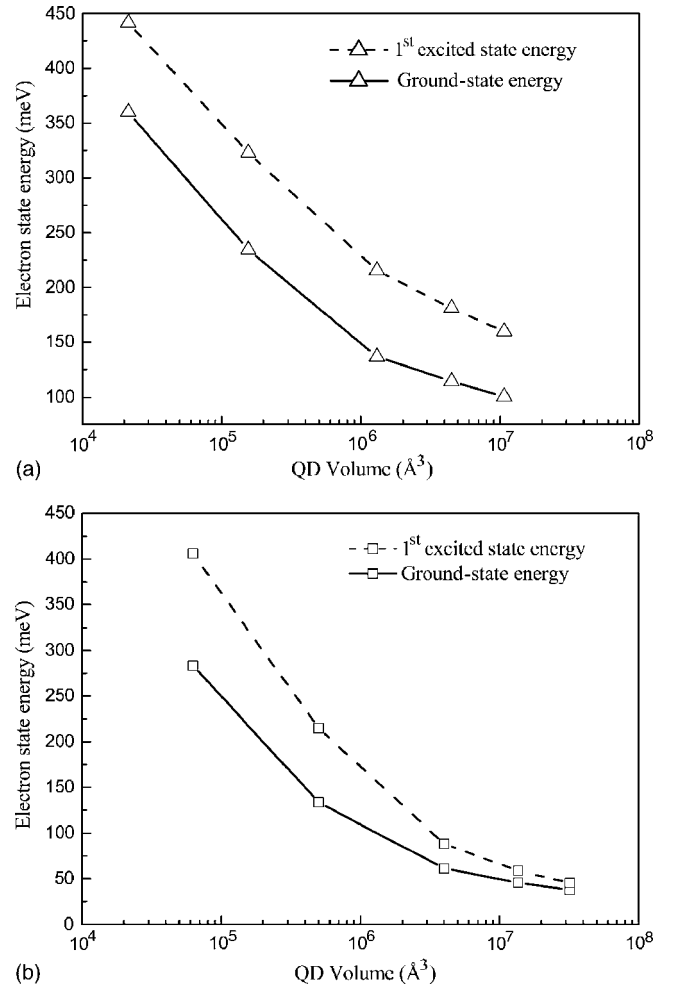


FIG. 2. Plot of electron ground-state energy and first excited-state energy of (a) PYRAMID and (b) CUBOID as function of QD volume. The lines are guides to the eyes.

have been reports on (truncated) pyramidal³¹ and lens-shaped³³ QDs taken by transmission electron microscopy (TEM). However, as reported in Ref. 31, conventional TEM is likely to show lens-shaped images even though the real QD shape is pyramidal. Only special imaging condition of the high-resolution TEM will show the real pyramidal shape. Therefore, to ensure we are comparing QD shapes with narrow tip to those of broad tip, we refer to a publication by Guzelian *et al.*³⁴ in which a comparison is made between spherical InAs colloidal QDs with pyramidal InAs QDs of comparable volume. Their results have shown that the photoluminescent (PL) energy peak of the spherical QDs of 52 Å diameter ($\sim 7.4 \times 10^4 \text{ Å}^3$) is ~ 80 meV lower than that of pyramidal QDs of similar volume. This agrees with our explanation of lower transition energy for QD shapes with broader tip. However, due to limitation of the colloidal QD growth process, we are unable to compare our work with experimental results for QDs larger than 60 Å diameter ($\sim 1.0 \times 10^5 \text{ Å}^3$).

Furthermore, our work is consistent with the calculations reported by Gunawan *et al.*¹ Although the effects we investigated are totally different from what they reported, their starting point with no interdiffusion is relevant to our work,

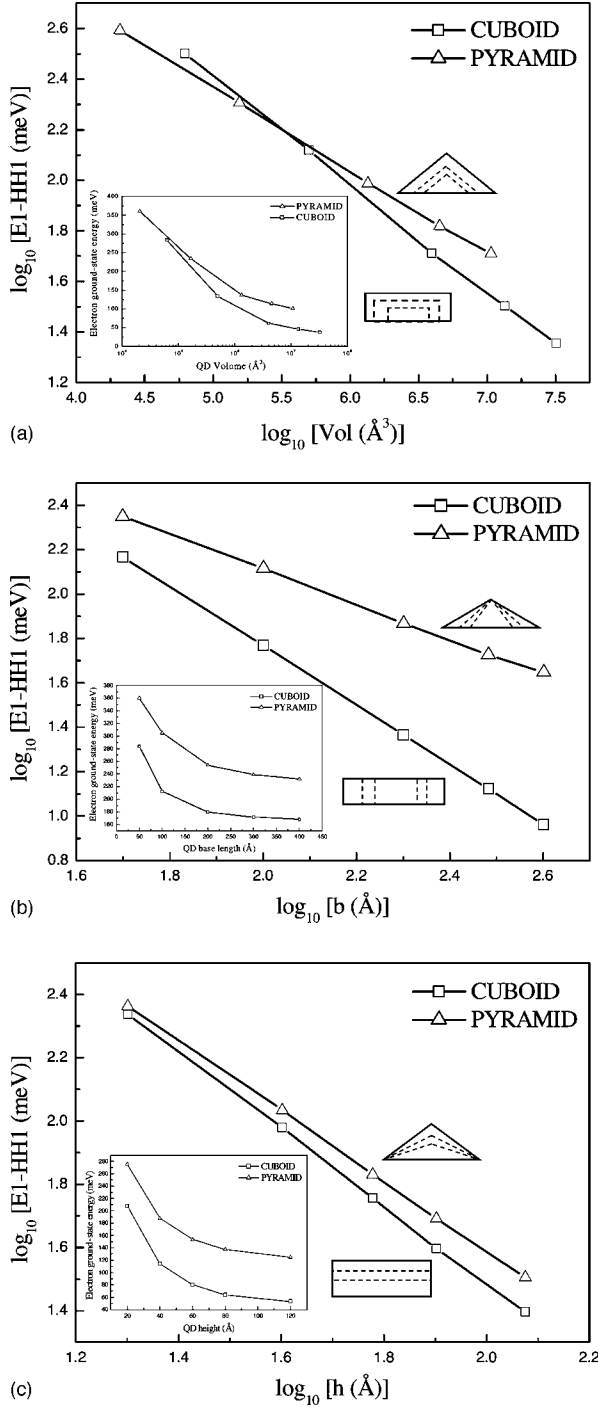


FIG. 3. Plot of normalized logarithm (base 10) graphs of PYRAMID and CUBOID for (a) volume, (b) base length, and (c) height dependencies. The lines are guides to the eyes. The abbreviation E1-HH1 denotes the ground-state energy. (Inset) Graphs of electron ground-state energy as function of (a) volume, (b) base length, and (c) height.

and it corresponds to a point on Fig. 1, i.e., volume of $\sim 1.67 \times 10^5 \text{\AA}^3$ with an aspect ratio of 0.5.

B. QD base length (height) variation

The increase in the QD volume, base length, or height results in decrease in the energy states due to reduction in the

TABLE V. Comparison of various $\gamma_{\text{Vol.}}$, γ_b , and γ_h for PYRAMID and CUBOID.

	PYRAMID	CUBOID
$\gamma_{\text{Vol.}}$	0.33 ^a , 0.32 ^b	0.43 ^a
γ_b	0.78 ^a	1.34 ^a
γ_h	1.10 ^a , 0.85 ^c	1.22 ^a , 0.95 ^d , 1.09 ^e

^aOur work.

^bReference 16.

^cReference 35.

^dReference 36, using single-particle pseudopotential plane-wave method.

^eReference 36, using many-particle configuration-interaction method.

confinement effect. However, comparing Eq. (A5) with Eqs. (A7) and (A8), the volume dependency $\gamma_{\text{Vol.}}$ and base length (height) dependency γ_b (γ_h) are significantly different; i.e., while $\gamma_{\text{Vol.}} \sim 0.67$, $\gamma_b = \gamma_h \sim 2$. This significant difference in the dependency can be used as a means to understand the QD formation process, i.e., whether addition of InAs coverage will result in increase of the volume or height (base length) of the QD.

To investigate this issue, we fitted our calculated results from the ground-state energy as function of volume, base length, and height and obtained values for $\gamma_{\text{Vol.}}^{\text{calc}}$, γ_b^{calc} , and γ_h^{calc} , respectively. The trend is again divided into two groups, namely, shapes with narrow tips and broad tips. Hence, for same reasons above, PYRAMID and CUBOID were chosen. The normalized logarithm (base 10) plots of PYRAMID and CUBOID for volume, base length, and height dependencies are shown in Figs. 3(a)–3(c), respectively. The dimension dependencies are seen from the gradients of the straight line graphs. The insets in Figs. 3(a)–3(c) show the electron ground-state energy as function of volume, base length, and height, respectively. Values of $\gamma_{\text{Vol.}}^{\text{calc}}$, γ_b^{calc} , and γ_h^{calc} for PYRAMID and CUBOID, together with results from others, are shown in Table V; and found to be lower than the ideal case of $\gamma_{\text{Vol.}} \sim 0.67$ and $\gamma_b = \gamma_h \sim 2$. This is due to finite energy barrier considered in the actual case and thus a smaller dependency on the dimensions. Hence, we expect the values of γ to approach that of the ideal case if the energy barrier is higher, e.g., by using AlGaAs instead of GaAs as the barrier layer.

Heitz *et al.*¹⁶ have demonstrated shell-like (onionlike) formation of Sb-surfactant mediated InAs/GaAs QD growth. It was shown that each monolayer of InAs coverage resulted in volume increment and not just height increment. We fitted the experimental PL data from their paper, and obtained a value for volume dependency $\gamma_{\text{Vol.}}^{\text{expt}} \sim 0.32$. This value agrees well with our calculated value of $\gamma_{\text{Vol.}}^{\text{calc}} \sim 0.33$. Furthermore, our calculated value of γ_h^{calc} was validated with data from Ref. 35, which considered optical properties of different QD heights with similar lateral size. A value of $\gamma_h^{\text{expt}} \sim 0.85$ was obtained by fitting to their experimental PL data. This value is lower than our calculated value of $\gamma_h^{\text{calc}} \sim 1.10$ since the barrier layer is InGaAs instead of GaAs. The lower energy barrier results in weaker height dependency compared to that of our work.

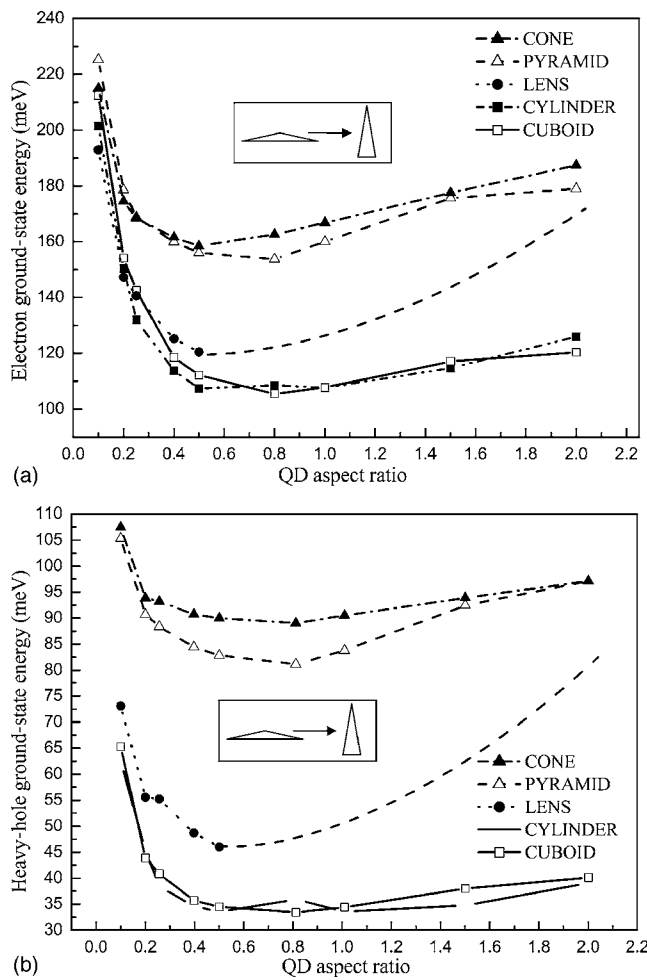


FIG. 4. Plot of (a) electron ground-state energy and (b) heavy-hole ground-state energy as function of QD aspect ratio, for various QD shapes (QD volume fixed at $8 \times 10^5 \text{ \AA}^3$). The predicted trend (dashed line) of the ground-state energy for $AR > 0.5$ is also included for LENS. The lines are guides to the eyes.

Narvaez *et al.*³⁶ reported calculations of the dependence of electronic structure of lens-shaped InGaAs QD as function of height. They compared values of γ_h calculated by the single-particle pseudopotential plane-wave method and many-body screened configuration-interaction (CI) approach. The values of γ_h were found to be 0.95 and 1.09, respectively. Both values of γ_h are lower than our calculated values ($\gamma_h^{\text{calc}} \sim 1.22$). This is because our calculation was based on InAs QD instead of InGaAs QD. Hence, the larger energy barrier resulted in stronger dependency compared to that of their work.

Most importantly, note that the energy dependencies are significantly different, i.e., γ_{Vol} is approximately three times smaller than γ_h (or γ_b). This large difference can be very useful for verification of QD formation. For example, if we increase the QD coverage in succession and find similar increase in the volume of the uncapped QD, we can check whether there is similar volume increment in the capped QD by taking PL measurements of the capped ones, plotting the logarithm (base 10) plot similar to ours, and obtaining the energy dependency γ_{Vol} from the gradient. Hence, by check-

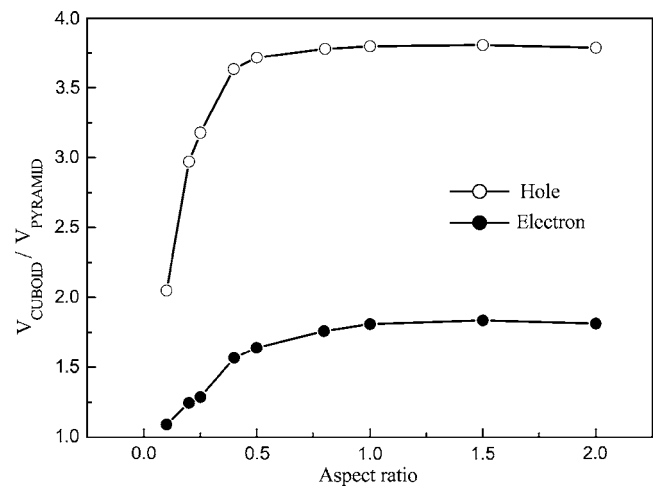


FIG. 5. Plot of the ratio of effective volume of CUBOID to that of PYRAMID for both electron and hole as function of aspect ratio. The lines are guides to the eyes.

ing whether the value of γ_{Vol} deviate significantly from that in Table IV, we can verify if the capped QD experienced a similar change as the uncapped ones.




Comparing with sophisticated tools like HREM, which requires longer turnaround time and sample preparation procedures, this method provides a relatively fast and inexpensive alternative to determine how much the capped QD had deviated from the uncapped ones upon growth parameter variation.

C. QD aspect ratio variation

Our calculated results of energy states as function of aspect ratio for different isovolume QD shapes are shown in Fig. 4. The energy states do not follow monotonic trends. Instead, there is an “optimum” aspect ratio for each QD shape where the energy state is the lowest. To understand the energy trend analytically, we derived Eq. (A9) in the Appendix. It is seen that the energy state exhibits two different trends: a steep decrease ($\sim AR^{-4/3}$) for smaller aspect ratio followed by a gentle, almost linear increase ($\sim AR^{2/3}$). The lowest ground-state energy is expressed in Eq. (A10) corresponding to an optimum aspect ratio of 1. The expression is derived for the ideal case of CUBOID QD with infinite energy barrier, and we have used it to explain the observed energy trend. We believe that, similar to $\gamma_{\text{Vol}}^{\text{calc}}$, γ_b^{calc} , and γ_h^{calc} , the aspect ratio dependency $\gamma_{\text{AR}}^{\text{calc}}$ will be smaller due to the finite energy barrier.

To explain the observed energy trend in Fig. 4 and results derived in the Appendix, we consider the competing effects of decrease in base length and increase in height, as aspect ratio increases. For smaller aspect ratio, decrease in confinement energy due to increase in height is much larger than increase in confinement energy due to decrease in base length. This explains the steep decrease in the ground-state energy following a small increase in aspect ratio. The inverse is also true for large increase in aspect ratio. However, the effect is smaller and the increase more gentle. When the effect due to the increase in height equals that due to the

TABLE VI. Illustration of different AR values (at fixed volume) for LENS.

AR \approx 0.1	AR \approx 0.5	AR \approx 2.0
		

decrease in base length, the lowest ground-state energy was obtained, i.e., the optimum aspect ratio AR_{opt} is reached. As a result, the QD energy is height dominant before AR_{opt} and base-length dominant after that. Since γ_h^{calc} is larger (smaller) than γ_b^{calc} for PYRAMID (CUBOID); indicating shapes with narrow (broad) tips have stronger (weaker) height dependency, we expect shapes with broad tips to reach the optimum aspect ratio faster than those with narrow tips.

In addition to the observed energy trend, there exists an obvious energy difference between shapes with narrow and broad tips. This is due to different effective volumes among the various shapes. This volume dependency on E_0 can be seen from Eq. (A9). Hence, for a given aspect ratio, $E_0 \sim V_{\text{eff}}^{-2/3}$ (e.g., $E_{0,\text{PYRAMID}} \sim V_{\text{eff,PYRAMID}}^{-2/3}$ and $E_{0,\text{CUBOID}} \sim V_{\text{eff,CUBOID}}^{-2/3}$), where V_{eff} is the effective volume of a particular shape. Taking the ratio of the energy at a particular aspect ratio and rearranging it, we obtain $V_{\text{eff,CUBOID}}/V_{\text{eff,PYRAMID}} = (E_{0,\text{PYRAMID}}/E_{0,\text{CUBOID}})^{3/2}$. Thus, the ratio of energy of various shapes provides us a direct means to quantify the ratio of (effective) volume seen by both electrons and holes. Therefore, by considering $E_{0,\text{PYRAMID}}/E_{0,\text{CUBOID}}$ from Fig. 4, the ratio of effective volume of electrons and holes as function of aspect ratio is plotted in Fig. 5. Indeed, $V_{\text{eff,CUBOID}}/V_{\text{eff,PYRAMID}} > 1$ throughout the aspect ratio variation considered in our work. This justifies the explanation of a larger effective volume for shapes with broad tips. The difference in the effective volume seen by both carriers is attributed to the different effective masses and confining potentials. Initial increase of $V_{\text{eff,CUBOID}}/V_{\text{eff,PYRAMID}}$ is due to larger increase in effective volume for the broad tip shapes; while the almost constant ratio of the volume after ~ 0.5 implies that carriers in both shapes see similar changes in the effective volume of the QD, with $V_{\text{eff,CUBOID}}$ always larger than $V_{\text{eff,PYRAMID}}$.

Note that computation for aspect/ratio > 0.5 was not performed for lens-shaped QDs (LENS) since the boundary condition defined only caters for $AR \leq 0.5$, i.e., only up to the point when the lens-shaped QDs become hemispherical QDs. However, we predict that there will be a transition from the “lower energy” group to the “higher energy” group as the aspect ratio increases beyond 0.5. This is due to transition of the lens-shaped tip from rounded to pointed one, as illustrated in Table VI. The predicted trend of LENS for aspect ratio > 0.5 is shown in Fig. 4.

Due to the low aspect ratio of most InAs QDs reported in current literature, increasing the aspect ratio (or height) seems to be the obvious way to redshift the transition energy. This is due to the smaller QD height of ~ 5 nm as compared to the base of ~ 24 nm.³⁷ Hence, a slight increase in the vertical dimension is sufficient to produce a significant reduction in the confinement energy. However, as the current

QD aspect ratio is ~ 0.1 – 0.3 , we are unable to find any reported experimental result with larger aspect ratio of ~ 1.0 to validate our calculations. Nevertheless, knowing that templated growth³⁸ and growth parameters variations^{39,40} do have an effect on the size, shape, and aspect ratio of QDs, the results in Fig. 4 will provide valuable insight into the energy trends for QD of different shapes.

We do not deny that more sophisticated models, e.g., the eight-band $k \cdot p$ model, will be needed for accurate representation of the full energy spectra, i.e., the correct energy calculation of the excited states. However, the focus of this paper is in the calculation of the confined ground-state energies and it is thus important to point out that simple single-band, effective mass model is sufficient for the calculation of the confined ground-state energy.^{6,10} Currently, a lot of input parameters of the involved bulk materials are still unknown. While parameters such as the fundamental energy gap, spin-orbit energy, and Γ -point conduction band mass are well known from experiments; the band gap deformation potential and band offsets are more difficult to determine. Therefore, even the most detailed QD energy calculations will suffer from the lack of knowledge of the essential input parameters. In fact, with proper choice of the input parameters, simple single-band, effective mass model can accurately calculate the ground-state energy.¹² As mentioned in our work, the consistency of our work with theoretical^{1,23,28,36} and experimental^{16,34,35} results of others thus justified the approximations and parameters used in our calculations.

IV. CONCLUSIONS

This paper reports a strained-modified, single-band, constant-potential three-dimensional model to study the dependence of electronic states of InAs/GaAs quantum dots (QDs) of different shapes and sizes. Our calculations were found to be consistent with experimental results and atomistic calculations from current literature. Our results can be summarized as follows: (i) monotonically decreasing energy trends with increasing QD size, i.e., $E \sim \text{size}^{-\gamma}$; (ii) smaller effective volume for QD shapes with narrow tips; (iii) energy dependency γ was approximately three times larger for base length (height) variation than volume variation; (iv) non-monotonic energy trends for all QD shapes as function of aspect ratio; (v) prediction of smaller optimum aspect ratio for QD shapes with broad tips; (vi) ratio of effective volume of both shapes ($V_{\text{eff,CUBOID}}/V_{\text{eff,PYRAMID}}$) was found to vary with aspect ratio; and (vii) prediction of a “crossover” from “lower energy” to “higher energy” group for lens-shaped QDs. As discussed, the difference in the energy dependency γ as function of base length (height) and volume can be used as an easier alternative to check on how much the capped QD had deviated in size from the uncapped ones. This will provide a faster and relatively inexpensive feedback loop, as compared to the use of more sophisticated tools, for growth experimentalists. In addition, the calculated energy trend as function of aspect ratio will provide valuable insight for QDs with higher than normal (> 0.5) aspect ratio.

ACKNOWLEDGMENTS

The authors are grateful to S. Y. Lee, W. K. Loke, and

C. Z. Tong for their comments and discussions. This project is partially supported by funding under the A*STAR ONFIG-II project.

APPENDIX

In this section, we present the expressions for the energy dependence on the size variation that was discussed in this paper. The expressions below are derived based on the ideal case of a square-based cuboid quantum dot with infinite potential barrier. The abbreviation used is the same as that described in Table II.

For the case of a square-based cuboid with base length b and height h , we can write the confinement energy as

$$E_{n_x, n_y, n_z} = \frac{\pi^2 \hbar^2}{2m^*} \left(\frac{n_x^2}{b^2} + \frac{n_y^2}{b^2} + \frac{n_z^2}{h^2} \right), \quad (\text{A1})$$

and the energy spacing as

$$\Delta E = \frac{\pi^2 \hbar^2}{2m^*} \left(\frac{n_x'^2 - n_x^2}{b^2} + \frac{n_y'^2 - n_y^2}{b^2} + \frac{n_z'^2 - n_z^2}{h^2} \right). \quad (\text{A2})$$

Therefore, the ground-state energy (i.e., $n_x = n_y = n_z = 1$) is

$$E_0 = \frac{\pi^2 \hbar^2}{2m^*} \left(\frac{2}{b^2} + \frac{1}{h^2} \right), \quad (\text{A3})$$

and the energy spacing from the first excited-state energy is

$$\Delta E = \frac{\pi^2 \hbar^2}{2m^*} \left(\frac{3}{b^2} \right), \quad (\text{A4})$$

since the height h is much smaller as compared to the base length b .

For the case of volume variation with constant aspect ratio of 0.5,

$$E_0^{\text{Vol}} = \frac{3\pi^2 \hbar^2}{4m^*} \left(\frac{\text{Vol.}}{4} \right)^{-2/3}, \quad (\text{A5})$$

$$\Delta E^{\text{Vol}} = \frac{3\pi^2 \hbar^2}{2m^*} (2\text{Vol.})^{-2/3}, \quad (\text{A6})$$

where $b=2h$, E_0^{Vol} and ΔE^{Vol} are the ground-state energy and energy spacing due to volume variation, respectively.

For the case of base length variation with constant height h_0 ,

$$E_0^b = \frac{\pi^2 \hbar^2}{2m^*} \left(\frac{2}{b^2} + \frac{1}{h_0^2} \right), \quad (\text{A7})$$

where E_0^b is the ground-state energy due to base length variation.

Similarly, for the case of height variation with constant base length b_0 ,

$$E_0^h = \frac{\pi^2 \hbar^2}{2m^*} \left(\frac{2}{b_0^2} + \frac{1}{h^2} \right), \quad (\text{A8})$$

where E_0^h is the ground-state energy due to height variation.

For the case of aspect ratio variation with constant volume V_0 ,

$$E_0^{\text{AR}} = \frac{\pi^2 \hbar^2}{2m^*} V_0^{-2/3} (\text{AR}^{-4/3} + 2\text{AR}^{2/3}), \quad (\text{A9})$$

where E_0^{AR} is the ground-state energy due to aspect ratio variation.

In this case, the energy does not follow a monotonic trend. For smaller AR value, it exhibits an AR dependency of $-4/3$; for larger AR value, it exhibits an AR dependency of $2/3$. Graphically, it means that there will be a sharp decrease in energy as the AR starts to increase from a small value (~ 0.1), and it approaches a gentle and almost linear increase as the AR becomes larger.

In addition, the lowest ground-state energy is

$$E_{0,\min} = \frac{3\pi^2 \hbar^2}{2m^*} V_0^{-2/3}, \quad (\text{A10})$$

and the corresponding aspect ratio is $\text{AR}_0 = 1$.

Note from Eq. (A10) that the minimum ground-state energy is (effective) volume dependent.

¹O. Gunawan, H. S. Djie, and B. S. Ooi, Phys. Rev. B **71**, 205319 (2005).

²S. S. Li, J. B. Xia, Z. L. Yuan, Z. Y. Xu, W. Ge, X. R. Wang, Y. Wang, J. Wang, and L. L. Chang, Phys. Rev. B **54**, 11575 (1996).

³C. A. Duque, N. Porras-Montenegro, Z. Barticevic, M. Pacheco, and L. E. Oliveira, Microelectron. Eng. **36**, 231 (2005).

⁴R. V. N. Melnik and K. N. Zotsenko, Modell. Simul. Mater. Sci. Eng. **12**, 465 (2004).

⁵H. Jiang and J. Singh, Appl. Phys. Lett. **71**, 3239 (1997).

⁶H. Jiang and J. Singh, Phys. Rev. B **56**, 4696 (1997).

⁷C. Pryor, Phys. Rev. B **57**, 7190 (1998).

⁸O. Stier, M. Grundmann, and D. Bimberg, Phys. Rev. B **59**, 5688 (1999).

⁹A. J. Williamson and A. Zunger, Phys. Rev. B **59**, 15819 (1999).

¹⁰C. Pryor, Phys. Rev. B **60**, 2869 (1999).

¹¹L. W. Wang, A. J. Williamson, A. Zunger, H. Jiang, and J. Singh, Appl. Phys. Lett. **76**, 339 (2000).

¹²M. Califano and P. Harrison, Phys. Rev. B **61**, 10959 (2000).

¹³D. Pal, V. G. Stoleru, E. Towe, and D. Firsov, Jpn. J. Appl. Phys. **41**, 482 (2002).

¹⁴V. G. Stoleru, D. Pal, and E. Towe, Physica E **15**, 131 (2002).

¹⁵W. D. Sheng and J. P. Leburton, Phys. Status Solidi B **237**, 394 (2003).

¹⁶R. Heitz, F. Guffarth, K. Potschke, A. Schliwa, D. Bimberg, N. D. Zakharov, and P. Werner, Phys. Rev. B **71**, 045325 (2005).

¹⁷B. Liu, Q. D. Zhuang, S. F. Yoon, J. H. Dai, M. Y. Kong, Y. P. Zeng, J. M. Li, L. Y. Lin, and H. J. Zhang, Int. J. Mod. Phys. B **15**, 1959 (2001).

¹⁸J. Shumway, A. J. Williamson, A. Zunger, A. Passaseo, M. De-

- Giorgi, R. Cingolani, M. Catalano, and P. Crozier, *Phys. Rev. B* **64**, 125302 (2001).
- ¹⁹R. V. N. Melnik and M. Willatzen, *Nanotechnology* **15**, 1 (2004).
- ²⁰D. Leonard, K. Pond, and P. M. Petroff, *Phys. Rev. B* **50**, 11687 (1994).
- ²¹M. Fricke, A. Lorke, J. P. Kotthaus, G. Medeiros-Ribeiro, and P. M. Petroff, *Europhys. Lett.* **36**, 197 (1996).
- ²²A. J. Williamson, L. W. Wang, and A. Zunger, *Phys. Rev. B* **62**, 12963 (2000).
- ²³M. A. Cusack, P. R. Briddon, and M. Jaros, *Phys. Rev. B* **54**, R2300 (1996).
- ²⁴F. Adler, M. Geiger, A. Bauknecht, F. Scholz, H. Schweizer, M. H. Pilkuhn, B. Ohnesorge, and A. Forchel, *J. Appl. Phys.* **80**, 4019 (1996).
- ²⁵A. M. Elabsy, *Phys. Scr.* **48**, 376 (1993).
- ²⁶S. H. Wei and A. Zunger, *Phys. Rev. B* **60**, 5404 (1999).
- ²⁷B. S. Ma, X. D. Wang, F. H. Su, Z. L. Fang, K. Ding, Z. C. Niu, and G. H. Li, *J. Appl. Phys.* **95**, 933 (2004).
- ²⁸M. Grundmann, O. Stier, and D. Bimberg, *Phys. Rev. B* **52**, 11969 (1995).
- ²⁹M. A. Cusack, P. R. Briddon, and M. Jaros, *Phys. Rev. B* **56**, 4047 (1997).
- ³⁰A. L. Efros, *Sov. Phys. Semicond.* **16**, 772 (1982).
- ³¹D. Bimberg, M. Grundmann, and N. N. Ledentsov, *Quantum Dot Heterostructures*, (Wiley, Chichester, 1999).
- ³²A. D. Andreev, J. R. Downes, D. A. Faux, and E. P. O'Reilly, *J. Appl. Phys.* **86**, 297 (1999).
- ³³X. Z. Liao, J. Zou, X. F. Duan, D. J. H. Cockayne, R. Leon, and C. Lobo, *Phys. Rev. B* **58**, R4235 (1998).
- ³⁴A. A. Guzelian, U. Banin, A. V. Kadavanich, X. Peng, and A. P. Alivisatos, *Appl. Phys. Lett.* **69**, 1432 (1996).
- ³⁵Jin Soo Kim, Phil Won Yu, Joo In Lee, Jong Su Kim, Song Gang Kim, Jae-Young Leem, and Minhyon Jeon, *Appl. Phys. Lett.* **80**, 4714 (2002).
- ³⁶G. A. Narvaez, G. Bester, and A. Zunger, *J. Appl. Phys.* **98**, 043708 (2005).
- ³⁷M. C. Xu, Y. Temko, T. Suzuki, and K. Jacobi, *J. Appl. Phys.* **98**, 083525 (2005).
- ³⁸A. Rastelli, S. Stufler, A. Schliwa, R. Songmuang, C. Manzano, G. Costantini, K. Kern, A. Zrenner, D. Bimberg, and O. G. Schmidt, *Phys. Rev. Lett.* **92**, 166104 (2004).
- ³⁹Hideaki Saito, Kenichi Nishi, and Shigeo Suguo, *Appl. Phys. Lett.* **74**, 1224 (1999).
- ⁴⁰P. B. Joyce, T. J. Krzyzewski, G. R. Bell, T. S. Jones, S. Malik, D. Childs, and R. Murray, *Phys. Rev. B* **62**, 10891 (2000).